Mitigation of MMC High-Frequency Oscillations by Wideband Passivation

Pengxiang Huang and Luigi Vanfretti

Depart. Electrical, Computer, and Systems Engineering

Rensselaer Polytechnic Institute

Troy, NY, 12180, U.S.A

huangp2@rpi.edu, vanfrl@rpi.edu

Abstract—**Modular multilevel converters are known to develop high-frequency oscillations (HFOs) with the power system they are connected to, and the root cause is that the system resonance frequencies fall into the delay-induced non-passive region of MMCs. To damp such oscillations, this paper presents a wideband passivation method that can shape the MMC impedance to become completely passive above 100 Hz. This work involves a systematic design approach for using voltage feedforward for passivizing an MMC inverter impedance, and using current feedforward for passivizing MMC rectifier impedance. The effectiveness of the proposed wideband passivation method is verified first by frequency-domain analysis and then validated via EMT simulations.**

Index Terms—**MMC control, high-frequency oscillation, active damping, wideband, passivity, control delay**

I. INTRODUCTION

WITH the rapidly growing use of modular multilevel converters (MMCs) in power systems for applications such as renewable energy integration [1], high-voltage dc (HVdc) transmission [2] and medium-voltage dc (MVdc) distribution [3], high-frequency oscillation (HFO) events have been reported as critical performance issues that need to be addressed [4]. HFOs are attributed to the delay-induced non-passive characteristic (i.e., negative damping) captured by the MMC impedance. Such HFOs can appear at any frequency from 100 Hz to the Nyquist frequency, and may exist at more than one frequency at a time [5], which brings challenges to stable system operation and damping control design [6]. Existing active damping methods can be broadly categorized as wideband filtering method [7] and narrowband damping method [5]. Wideband filtering inserts lowpass filters (LPFs) into existing control loops, which can effectively eliminate the negative damping over a wide frequency range. However, it often leads to deteriorated MMC damping performance in the region under the corner frequency of the LPF. In a practical system, varying in MMC operating conditions and system topology can change the HFO frequencies, resulting in new excited oscillations in the frequency range below the corner frequency of the LPF. On the other hand, narrowband damping method places a damping function combined with a bandpass filter (BPF) in parallel with existing controllers, and can selectively add positive damping to the MMC impedance around frequencies of concern. However, the narrowband

damping function should be used in conjunction with online resonance detection and adaptive damping design in order to ensure an effective and robust suppression of HFOs [6], which inevitably increases the complexity of integrating online detection capability with precise damping tuning.

Considering the above-mentioned limitations of both wideband filtering and narrowband damping approaches in suppressing HFOs, this paper introduces a wideband active damping method capable of canceling out the delay-induced negative damping of MMC impedance. The wideband damping is realized by feedforwarding either ac current or voltage through a feedforward compensator, and then incorporating the output signal into the modulation signals of the MMC. This method ensures the MMC impedance to achieve complete passivity above 100 Hz, and therefore is termed as "wideband passivation method" in this work.

The reminder of this paper is organized as follows. Section II describes the system under study. Section III present a systematic design approach to develop the wideband passivation term for MMC in ac current-control mode (MMC inverter) and MMC in ac voltage-control mode (MMC rectifier). Section V demonstrates the efficacy of the proposed wideband passivation method through frequency-domain impedance sweep and by conducting EMT simulations in two different MMC-based HVDC systems. Section VI concludes this paper.
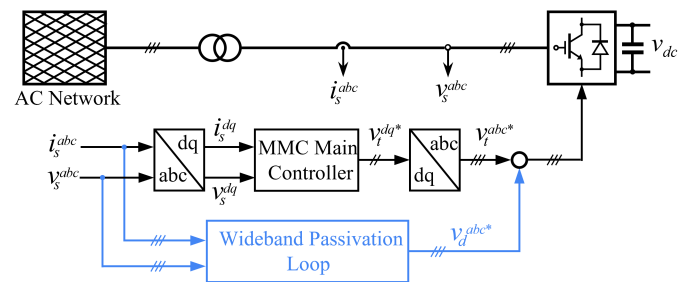
II. MMC-BASED SYSTEM UNDER STUDY

Fig. 1. Schematic of the system under study.

Figure 1 shows a schematic of the MMC-based system under study, which also indicates where the proposed wideband passivation loop should be introduced. In such configuration,

the MMC can be treated as either an inverter or rectifier. On the other hand, the ac network can be either a passive grid (i.e., overhead lines/cables) or a wind farm connected to an MMC terminal as part of a broader interconnection (e.g. via HVdc). In this work, an MMC inverter with unity power factor and an MMC rectifier with single-loop ac voltage control (i.e., ac current inner loop is ignored) are considered as the examples for designing wideband passivation. However, the proposed wideband passiviation method can also be extended to MMCs operating in other control modes. In addition, since this paper targets the frequency range from 100 Hz to the Nyquist frequency, the simplified impedance model of MMC [8] can be used to design and test the proposed wideband passivation method. The simplified impedance models of an MMC inverter and rectifier are given by

$$Z_{Inv}(s) = sL + e^{-sT_d}(H_i(s - j\omega_1) - jK_d) \tag{1a}$$

$$Z_{Rec}(s) = sL/[1 + e^{-sT_d}H_v(s - j\omega_1)] \tag{1b}$$

where L is half of MMC arm inductance; e^{-sT_d} represents a lumped time delay effect; $H_i(s - j\omega_1)$ represents the ac current control function in dq-reference frame and K_d is its current decoupling gain; $H_v(s - j\omega_1)$ represents the ac voltage control function in dq-reference frame. The subscript Inv and Rec indicates the inverter and rectifier, respectively.

III. MMC PASSIVATION METHODOLOGY

The passivation method discussed in this paper is based on adding a feedforward compensator in parallel (in blue in Fig. 1) with existing MMC controllers to make the MMC impedance equal or approximate to sL (i.e, fully passive) in the high-frequency range. It is known that the use of current feedforward introduces a term to the numerator of the MMC impedance, while the use of voltage feedforward introduces a term to the denominator [5], thus a passivized impedance of an MMC inverter and an MMC rectifier are expressed as

$$Z_{Inv}^{PD}(s) = \frac{sL + e^{-sT_d}[H_i(s - j\omega_1) - jK_d + y_i(s)]}{1 + e^{-sT_d}y_v(s)} \tag{2a}$$

$$Z_{Rec}^{PD}(s) = \frac{sL + e^{-sT_d}y_i(s)}{1 + e^{-sT_d}[H_v(s - j\omega_1) + y_v(s)]} \tag{2b}$$

where the superscript PD means "passivized", while $y_i(s)$ and $y_v(s)$ represent transfer functions of the current feedforward and voltage feedforward compensators for passivation, respectively. Note that either current or voltage feedforward terms can be used to passivize the MMC impedance in the high-frequency range, therefore $y_i(s)$ and $y_v(s)$ are such that exactly one of them is zero.

A. Passivity-based Design of Feedforward for MMC Inverter

1) Current Feedforward Term

The current feedforward terms $y_i(s)$ for the passivation of MMC inverter can be obtained by solving the following equation

$$Z_{Inv}^{PD}(s)|_{y_v(s)=0} = sL \tag{3}$$

which yields $y_i(s)$ as expressed by

$$y_i(s) = -H_i(s - j\omega_1) + jK_d \tag{4a}$$

$$\tilde{y}_i(s) = \frac{s^2}{s^2 + 2\pi s + (2\pi f_{ch})^2}[-H_i(s - j\omega_1) + jK_d]. \tag{4b}$$

Observe that from (4a), $y_i(s)$ essentially completely eliminates the current control effects, which would deteriorate the transient dynamics of current control loop and may also jeopardize MMC's low-frequency stability. To remove the unwanted effects from $y_i(s)$ in the low-frequency range, a high-pass filter can be added, resulting in the modified expression shown in (4b). However, the high-pass filter introduces phase lag to $\tilde{y}_i(s)$ below its corner frequency f_{ch}. This phase lag worsens the negative damping of MMC in the frequency range below f_{ch}, making it impossible to fully passivize the MMC inverter using $y_i(s)$. Therefore, passivation of the MMC inverter via current feedforward will not be further elaborated in this paper.

2) Voltage Feedforward Term

The voltage feedforward terms $y_v(s)$ for the passivation of an MMC inverter can be obtained by solving

$$Z_{Inv}^{PD}(s)|_{y_i(s)=0} = sL \tag{5}$$

which results in $y_v(s)$ as expressed by the following equation

$$y_v(s) = \frac{1}{s}\left(\frac{K_{pi}}{L} + \frac{K_{ii}}{L}\frac{1}{s - j\omega_1} - j\frac{K_d}{L}\right) \tag{6}$$

where K_{pi} and K_{ii} are the proportional and integral gains of the ac current controller, and $1/s$ represents the integration of the PCC voltage of the MMC. Substituting (6) and $y_i(s) = 0$ into (2a), the resulting passivized impedance of MMC inverter becomes sL and the current controller is not modified.

As can be seen from (6), $1/(s - j\omega_1)$ contains a frequency shift $-j\omega_1$, which can be realized either by placing the integrator in dq-reference frame or by ROGI function [12]. On the other hand, jK_d/L creates a 90° phase rotation to the input voltage signal, which requires its implementation in either the dq- or $\alpha\beta$-reference frames as a cross-coupling term.

3) Implementation Consideration for $y_v(s)$

Observe that (6) requires the implementation of an integrator in the abc-stationary frame and one integrator in dq (or $\alpha\beta$)-reference frame. As mentioned in [10], the integrator would amplify the small dc-offset caused by a voltage sensor, which may lead to the saturation of integrator or instability of the converter. In addition, a dc-offset may also result from the initial value of the integrator, which is the product of: 1) input sinusoidal signals that are not at their peak when integration begins; or 2) a rapid change in the input signals, e.g., high-frequency unstable oscillations. Note, this dc-offset is known as the air-gap flux in a motor-drive systems [11].

To address this issue, the pure integrator is placed in cascade using a 1st-order highpass filter, which results in a low-pass filter-based approximation of the integrator

$$H_{LPF}(s) = \frac{1}{s}\frac{s}{s + 2\pi f_{cl}} = \frac{1}{s + 2\pi f_{cl}} \tag{7}$$
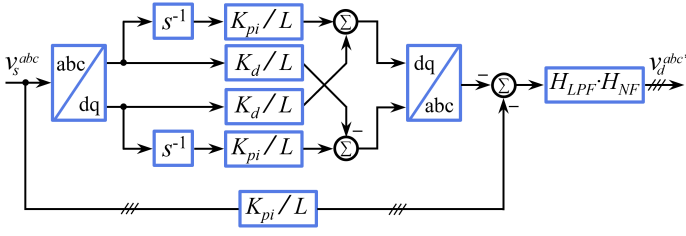
Fig. 2. Block diagram of wideband passivation for MMC inverter through voltage feedforward

where f_{cl} is the corner frequency of the lowpass filter. While the LPF can minimize the dc-offset, a small dc-offset may still remain at $1/(j2\pi f_{cl})$. It should be noted that using a low-pass filter (LPF) with a low f_{cl}, which provides a better approximation of a pure integrator, can result in degraded dc offset rejection in the feedforward voltage signal. Therefore, in this work, a value of 5 Hz is chosen for f_{cl} to balance this trade-off.

In addition, to avoid unintended effects at the fundamental frequency f_1, the feedforward output must be coupled with a highpass or notch filter to exclude fundamental frequency component from the feeforward loop. In order to avoid change the phase response of MMC impedance in both low- and high-frequency ranges, the following notch filter whose transfer function is shown in (8) is used

$$H_{NF}(s) = \frac{s^2 + (2\pi f_{cn})^2}{s^2 + 2\pi s + (2\pi f_{cn})^2}. \tag{8}$$

As a consequence, the actual implementation of $y_v(s)$ for the MMC inverter's passivation is expressed as

$$\hat{y}_v(s) = H_{NF}(s)H_{LPF}(s)(\bullet) \tag{9}$$

where $(\bullet)$ corresponds to the term in parenthesis of the R.H.S. in (6). Note that the only difference between (6) and (9) is that $1/s$ is replaced by $H_{NF}(s)H_{LPF}(s)$.

The block diagram of the passivation process through $y_v(s)$ is given in Fig. 2. As observed in Fig. 2, the integrator in the dq-reference frame is not approximated by $H_{LPF}(s)$. This is because leaving the zero-sequence signal uncontrolled inherently blocks the propagation of the dc offset in the ac voltage measurement from phase domain to dq-domain.

B. Passivity-based Design of Feedforward for MMC Rectifier

1) Voltage Feedforward Term

The voltage feedforward terms $y_v(s)$ for the passivation of an MMC operating as a rectifier can be obtained by solving the following equation

$$Z_{Rec}^{PD}(s)|_{y_i(s)=0} = sL \tag{10}$$

which yields $y_v(s)$ as expressed by

$$y_v(s) = -H_v(s - j\omega_1). \tag{11}$$

The cancellation of the ac voltage control loop by $y_v(s)$ can be observed in (11), and this could have a significant impact on the transient performance and stability of an MMC in the lower frequency range. Hence, this method will not be

further discussed in this paper. However, because the integral gain of $H_v(s - j\omega_1)$ has negligible influence on the MMC impedance at high-frequencies and ac voltage control typically excludes the decoupling terms in the dq-reference frame, a simple alternative is to modify (11) by setting $y_v(s) = -K_{pv}$, where K_{pv} is the proportional gain of $H_v(s - j\omega_1)$.

2) Current Feedforward Term

The current feedforward terms for the passivation of an MMC operating as a rectifier can be derived by solving

$$Z_{Rec}^{PD}(s)|_{y_v(s)=0} = sL \tag{12}$$

which yields $y_i(s)$ as

$$y_i(s) = s\left(K_{pv}L + \frac{K_{iv}L}{s - j\omega_1}\right) \approx sK_{pv}L + K_{iv}L \tag{13}$$

where K_{pv} and K_{iv} are the proportional and integral gains of the ac voltage compensator, respectively, and s represents the differentiation of ac voltage of the MMC rectifier. Note that $y_i(s)$ carries an integrator $1/(s - j\omega_1)$ represented in the dq-reference frame, which can be approximated by $1/s$ in the high-frequency range. As a result, $y_i(s)$ in (12) can be further simplified to be $(sK_{pv}L + K_{iv}L)$ (as shown in the R.H.S. of (13)), whose realization requires only one derivative block. It is worth noting that $(1/s)\cdot[1/(s - j\omega_1)]$ in (6) shall not be approximated as $1/s^2$ because both s and $(s - j\omega_1)$ are frequency-dependent.

3) Implementation Consideration for $y_i(s)$

It can be observed that (13) necessitates the use of a derivative block, which is not feasible to implement in a practical system. In addition, exact differentiation will inevitably cause unacceptable noise amplification. A highpass filter, given by (14), is thus used in this work to approximate the derivative block. The time constant τ in the denominator of $H_{HPF}(s)$ corresponds to the desired time constant of the derivative block

$$H_{HPF}(s) = \frac{s}{\tau s + 1}. \tag{14}$$

To select the value of τ, one can determine the desired corner frequency f_{ch} of $H_{HPF}(s)$ based on the damping range requirements and then set $\tau = 1/(2\pi \cdot f_{ch})$. In order to ensure the performance of differentiation below the Nyquist frequency, $\tau = 1/(2\pi \cdot 5000)$ is selected in this work.

As a consequence, the implementation of $y_i(s)$ for the MMC rectifier's passivation is expressed as

$$\hat{y}_i(s) = H_{HPF}(s)\left(K_{pv}L + \frac{K_{iv}L}{s - j\omega_1}\right) \tag{15}$$
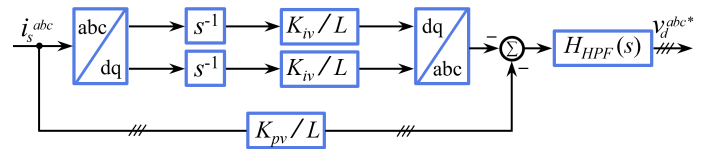

Fig. 3. Block diagram of wideband passivation for MMC rectifier through current feedforward

The block diagram of the passivation process through $y_i(s)$ is given in Fig. 3.

IV. VERIFICATION AND CASE STUDY

To evaluate the performance of the proposed wideband passivation method, this section first compares the analytical impedance responses of un-passivizedand passivized MMC with their numerical impedance scan performed on EMT models. The passivation loop design for the MMC inverter adheres to the principle outlined in Section III A *2)*, whereas the passivation loop design for the MMC rectifier follows Section III B *2)*. In addition, two MMC application examples are provided to further corroborate the efficacy of the proposed wideband passivation method. The key parameters of the MMCs and the design of the passivation loops used in this section are summarized as follows:

- MMC power stage: arm impedance = $(0.1 + j0.05)$ Ω; rated ac-side voltage = 300 kV; rate dc-side voltage = ± 320 kV; system frequency = 50 Hz.
- MMC inverter control: ac current loop bandwidth = 200 Hz; phase-locked loop bandwidth = 15 Hz. The phase margin of each loop is 45°; time delay = 200 μs.
- $\hat{y}_v(s)$ for MMC inverter: the corner frequency f_{cl} of H_{LPF} = 5 Hz; the corner frequency f_{cn} of H_{NF} = 5 Hz.
- MMC rectifier control: ac voltage loop bandwidth = 10 Hz; ac voltage loop phase margin is 120°; time delay = 200 μs.
- $\hat{y}_i(s)$ for MMC rectifier: the corner frequency f_{ch} of H_{HPF} = 5000 Hz.

A. Impedance Responses of the Passivized MMCs

1) Wideband Passivation Effect at High-Frequencies

Fig. 4 compares the un-passivizedimpedance of MMC inverter and rectifier with their passivized impedance, along with the numerical impedance scan results. The close correspondence between the numerical scans of passivized MMC impedances and the passivized impedances predicted by (2a), (2b) further validates the accuracy and rationality of using simplifed impedance model for designing wideband passivation. As clearly shown in Fig. 4, both the MMC inverter impedance and MMC rectifier impedance become fully passive from 100 Hz above after applying wideband passivation, which indicates that the proposed wideband passivation method is effective in eliminating the delay-induced negative damping of MMC. It is noteworthy that the zero-damping characteristic (i.e., exactly 90° phase response) of the passivized MMC above 100 Hz can be further compensated by the inherent resistances from the MMC arms, transformers at the PCC, as well as other passive filter devices placed at the MMC output terminal.

2) Wideband Passivation Effect at Low-Frequencies

To see the wideband passivation effect on low-frequency impedance response of MMC, Fig. 5 plots un-passivizedand passivized impedance of MMC inverter and rectifier, in which the impedance responses are calculated by full model. As evident from the comparison, the impedance is completely
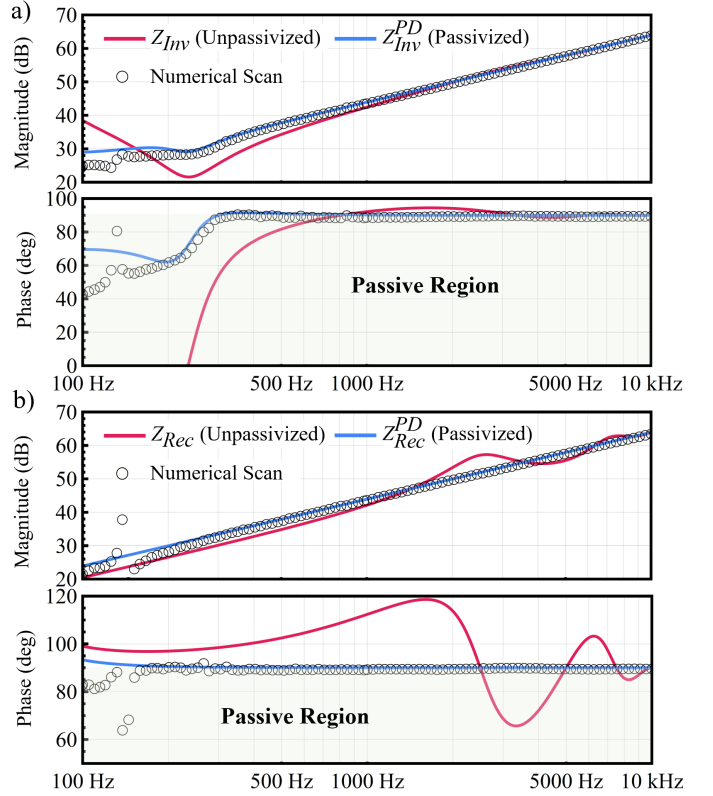

Fig. 4. Wideband passivation effect on high-frequency MMC impedance: a) $\hat{y}_v(s)$ effect on MMC inverter; b) $\hat{y}_i(s)$ effect on MMC rectifier
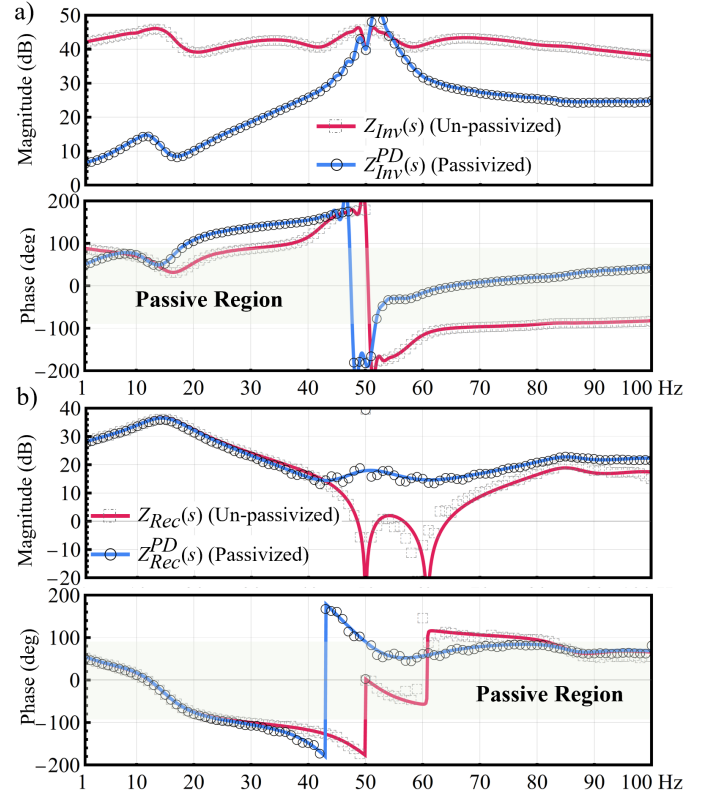

Fig. 5. Wideband passivation effect on low-frequency MMC impedance: a) $\hat{y}_v(s)$ effect on MMC inverter; b) $\hat{y}_i(s)$ effect on MMC rectifier

passivized for both MMC inverter and rectifier in the 50 Hz ~ 100 Hz range. Thus, there is no negative damping in this range, which helps MMC inverter and MMC rectifier in preventing any sub-synchronous oscillations (SSO) in such region.

The undesired effects of employing the proposed wideband passivation arises within the frequency range below the fundamental frequency, especially for MMC inverter. As indicated by Fig. 4 a), the wideband passivation results in an enlarged negative damping of MMC inverter within the 20~50 Hz frequency range, which may cause SSOs between the MMC inverter and a weak capacitive grid. To address this, a narrowband damping function [5] can be equipped with the wideband passiviation method. Conversely, the wideband passivation merely extends the negative damping of MMC recitifer to 30~40 Hz, while the impedance response below 30 Hz remains virtually unchanged.

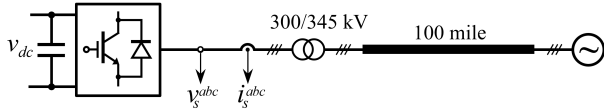### B. MMC Inverter Connected to Overhead Transmission Lines

Fig. 6. An MMC-based grid integration via a long OTL.

The first case study aims to verify the proposed method in a system involving an MMC inverter integrated to the ac grid by a 345 kV 100-mile overhead transmission line (OTL), and the single line diagram of the system is depicted in Fig. 6. In order to accurately model the behavior of long OTLs and demonstrate the HFO issues, the frequency-dependent phase model [13] of transmission line is used in this case study.

Fig. 7 compares the impedance responses of MMC without/with the proposed wideband passivation (marked by $Z_{Inv}(s)$ and $Z_{Inv}^{PD}(s)$) to the OTL impedance (marked by $Z_g(s)$). Of the multiple magnitude intersections between $Z_{Inv}(s)$ and $Z_g(s)$, the ones at 1551 Hz and 2450 Hz have 182° and 180° phase difference, respectively, indicating two unstable oscillations. With the proposed wideband passivation, the phase differences at the two intersection frequencies are reduced to 177° and 176°, signifying the mitigation of oscillations at both frequency. It should also be noted that the resistance of the transformer and overhead lines provides a level of positive damping to ensure the phase difference between $Z_{Inv}^{PD}(s)$ and $Z_g(s)$ smaller than 180°.

The effectiveness of such passivation loop is further confirmed by time-domain simulation results shown in Fig. 8. The wide passivation $\hat{y}_v(s)$ is initially disabled between $t = 0$ and $0.5\ s$, during which a growing oscillation dominated by the 1551 Hz resonance is observed. This unstable oscillation is mitigated when the wideband passivation $\hat{y}_v(s)$ is applied at $t = 0.5\ s$, and the MMC inverter can transfer power to the ac grid through the 100-mile OTL without stability issues. The unstable oscillation is shown again when $\hat{y}_v(s)$ is disconnected at $t = 2.5\ s$, which further demonstrates the effectiveness of the wideband passivation method.
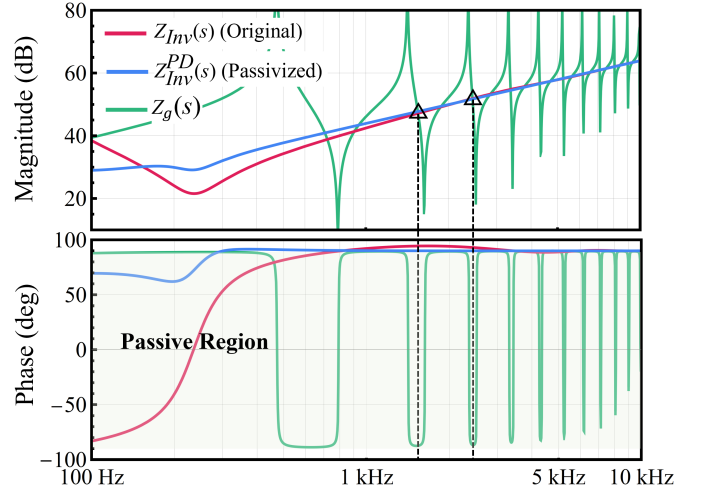

Fig. 7. Impedance response of: MMC inverter (red); MMC inverter passivized by $\hat{y}_v(s)$ (blue), and 100-mile OTL (green).
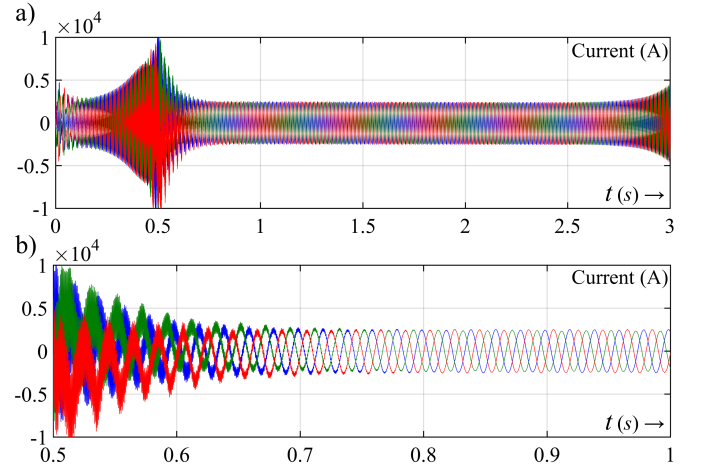

Fig. 8. Simulated time-domain responses of: a) overall MMC current responses; b) zoom-in view of MMC current between $0.5 \sim 1\ s$.

C. MMC Rectifier for Wind Farm Interconnection

The second case study aims to illustrate the proposed wideband passivation when used to suppress the oscillations between an MMC rectifier and a wind farm. The schematic diagram of the system is depicted in Fig. 9. In the wind farm, there are six 5-mile cable strings rated at 66 kV, and the terminal of each string is connected by an aggregated 150 MW Type-IV turbine interfaced via a 0.69/66 kV step-up transformer. Note that, 300 μs delay are included in the wind turbine controllers to create a negatively damped wind farm impedance in the medium frequency range. The six cable string are then collected, and the voltage is elevated from 66 kV to 300 kV in order to connect with the MMC rectifier at PCC.
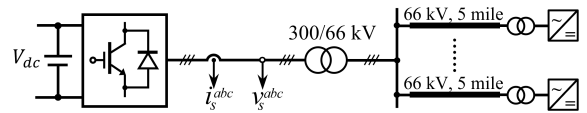

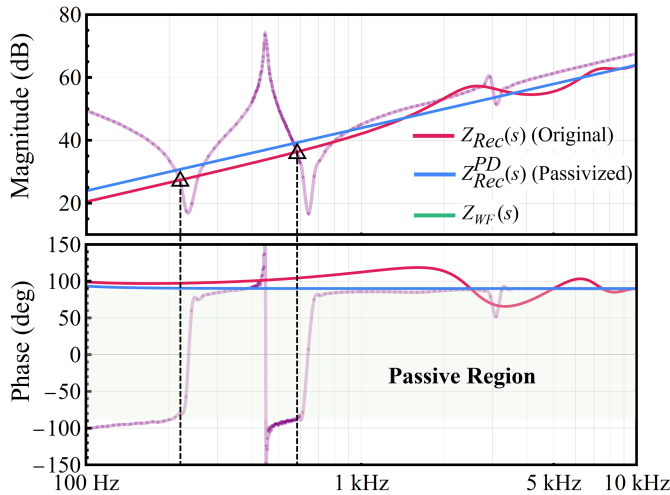Fig. 9. MMC-based wind integration through cable networks.

Fig. 10. Impedance responses of MMC rectifier (red) and its passivized impedance with $\hat{y}_i(s)$ (blue) against wind farm impedance (purple).

Fig. 11. Simulated time-domain responses of: a) overall MMC voltage responses; b) zoom-in view of the MMC voltage between $0.2 \sim 0.4\ s$.

Fig. 10 compares the output impedance of the MMC rectifier without/with the wideband passivation (marked by $Z_{Rec}(s)$ and $Z_{Rec}^{PD}(s)$) to the wind farm impedance (marked by $Z_{WF}(s)$) above 100 Hz. $Z_{Rec}(s)$ intersects with $Z_{WF}(s)$ at 218 Hz and 583 Hz, where the phase difference are 180.1° and 192.2°, respectively, indicating two unstable oscillations. As shown in Fig. 10, the passivation loop $\hat{y}_i(s)$ reshapes the $Z_{Rec}(s)$ to become passive above 100 Hz and moves the system resonance down to 210 Hz and 567 Hz where the phase difference between MMC rectifier and wind farm are 175.8° and 179.4°. The passivation is therefore expected to mitigate unstable oscillations at 583 Hz, while make the system poorly damped at 567 Hz due to the relatively small amount of positive net-damping.

The time-domain results are presented in Fig. 11, where the simulation starts without employing the proposed wideband passivation loop $\hat{y}_i(s)$ in the MMC rectifier. At $t = 0.2s$, the wind farm is connected to the MMC such that the unstable oscillation at 583 Hz is immediately excited. $\hat{y}_i(s)$ is then activated at $t = 0.2\ s$ and the fast-growing oscillation is suppressed. At $t = 1.8\ s$, $\hat{y}_i(s)$ is disabled and the resonance at 583 Hz grows again, indicating the efficacy of the passivation.

V. CONCLUSIONS

This study presented a widband passivation approach for suppressing high-frequency oscillations that may arise in MMC-based systems due to delay-induced non-passive characteristic of MMC. By incorporating the proposed wideband passivation loop in parallel with the MMC's existing controls, time delay effects are effectively eliminated from the output impedance of MMC above 100 Hz. The proposed wideband passivation complements the existing active damping method, providing an effective approach for MMC to avoid HFO issues when it is connected to the ac system.

REFERENCES

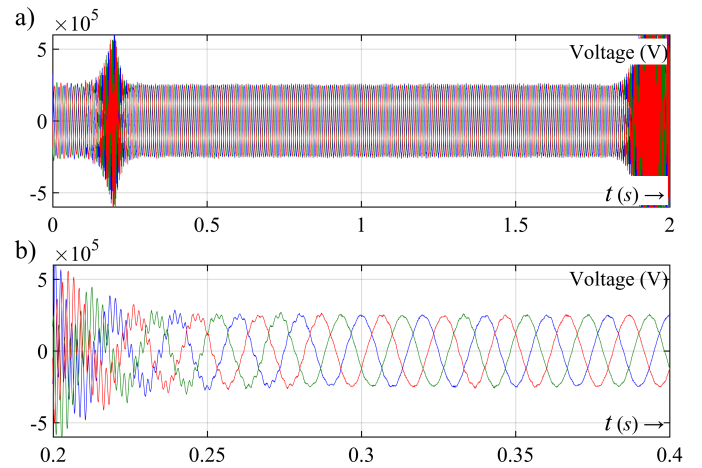[1] P. Huang and L. Vanfretti, "Analysis of Internal Energy in GFL-MMCs and a Decoupled Energy Control Scheme," *2023 IEEE Power & Energy Society Innovative Smart Grid Technologies Conference (ISGT)*, Washington, DC, USA, 2023, pp. 1-5.

[2] B. Yang, Z. He, H. Ma, H. Wang, Y. Lu, P. Qiu, P. Huang, "Fault isolation characteristics of the hybrid DC circuit breaker," *2017 IEEE Conference on Energy Internet and Energy System Integration (EI2)*, Beijing, China, 2017, pp. 1-6.

[3] J. Su, P. Dehghanian, B. Vergara and M. H. Kapourchali, "An Energy Management System for Joint Operation of Small-Scale Wind Turbines and Electric Thermal Storage in Isolated Microgrids," *2021 North American Power Symposium (NAPS)*, College Station, TX, USA, 2021, pp. 1-6.

[4] K. Ji et al., "A Hierarchical Small-Signal Controller Stability Analysis Method for the MMCs," in *IEEE Transactions on Power Delivery*, vol. 37, no. 4, pp. 2587-2598, Aug. 2022.

[5] P. Huang and J. Sun, "Mitigation of MMC High-Frequency Resonance by Narrowband Damping," *2021 IEEE 22nd Workshop on Control and Modelling of Power Electronics (COMPEL)*, Cartagena, Colombia, 2021, pp. 1-7.

[6] P. Huang and L. Vanfretti, "Adaptive Passivity Compensation of Grid-following MMC for Stable Grid Integration," *2022 IEEE Industry Applications Society Annual Meeting (IAS)*, Detroit, MI, USA, 2022, pp. 1-8.

[7] Y. Li, T. An, D. Zhang, X. Pei, K. Ji and G. Tang, "Analysis and Suppression Control of High Frequency Resonance for MMC-HVDC System," in *IEEE Transactions on Power Delivery*, vol. 36, no. 6, pp. 3867-3881, Dec. 2021.

[8] H. Wu, X. Wang, Ł. Kocewiak and L. Harnefors, "AC Impedance Modeling of Modular Multilevel Converters and Two-Level Voltage-Source Converters: Similarities and Differences," *2018 IEEE 19th Workshop on Control and Modeling for Power Electronics (COMPEL)*, Padua, Italy, 2018, pp. 1-8.

[9] K. Ji, H. Pang, Z. He, Y. Li, D. Liu and G. Tang, "Active/Passive Method-Based Hybrid High-Frequency Damping Design for MMCs," in *IEEE Journal of Emerging and Selected Topics in Power Electronics*, vol. 9, no. 5, pp. 6086-6098, Oct. 2021.

[10] H. Wu and X. Wang, "Virtual-Flux-Based Passivation of Current Control for Grid-Connected VSCs," in *IEEE Transactions on Power Electronics*, vol. 35, no. 12, pp. 12673-12677, Dec. 2020.

[11] R. Wu and G. R. Slemon, "A permanent magnet motor drive without a shaft sensor," in *IEEE Transactions on Industry Applications*, vol. 27, no. 5, pp. 1005-1011, Sept.-Oct. 1991.

[12] C. A. Busada, S. Gomez Jorge, A. E. Leon and J. A. Solsona, "Current Controller Based on Reduced Order Generalized Integrators for Distributed Generation Systems," in *IEEE Transactions on Industrial Electronics*, vol. 59, no. 7, pp. 2898-2909, July 2012.

[13] W. S. Meyer and H. W. Dommel, "Numerical Modelling of Frequency-Dependent Transmission-Line Parameters in an Electromagnetic Transients Program," in *IEEE Transactions on Power Apparatus and Systems*, vol. PAS-93, no. 5, pp. 1401-1409, Sept. 1974.